# HiFFUT - A New Class of Transducer

Update Report 2

Dr Andrew Feeney MEng(Hons) PhD CEng MIMechE

Research Fellow in the Centre for Industrial Ultrasonics

Department of Physics

University of Warwick

Coventry CV4 7AL, United Kingdom

a.feeney@warwick.ac.uk

Website: www2.warwick.ac.uk/fac/sci/physics/research/ultra/research/hiffut

September 18, 2017

WARWICK
THE UNIVERSITY OF WARWICK

# Contents

# List of Figures

# List of Tables

# General Overview

This report is provided as an update of the HiFFUT research project up to September 2017. Included in this report are details of the next stage of the investigation of the electro-mechanical behaviour of flexural transducers, with analysis of the nonlinear dynamic response of flexural ultrasonic transducers for different excitation vibration amplitudes. Further information regarding the pressure vessel design and fabrication and the progress in the development of high-frequency and high-temperature flexural transducers are also included.

An on-line tool allowing anyone to design a HiFFUT cap membrane was developed using JavaScript on an HTML interface, and is now available on the project web-site, the link for which is provided on the title page of this report. The user can enter desired dimensions, comprising diameter and thickness, choose from a list of materials comprising aluminium, stainless steel, and titanium, and finally designate the axisymmetric mode of vibration of interest, either (0,0), (1,0) or (2,0). The operating mode frequency is then computed in terms of kHz to three decimal places. An example of the graphical user interface is shown in Figure 1.


## HiFFUT Design Tool

This section provides an expedient and rapid estimator for basic HiFFUT design and operating parameters, for the fundamental axisymmetric operating modes of vibration, and for three common cap materials. This is a predictor based on the vibration modes of an edge-clamped plate, and should be used as a guideline only, since physical device parameters will affect the vibration characteristics of a HiFFUT. The predictor makes use of the equations presented above to generate the operating frequency in each case, and take account of the rigidity of the cap membrane. The higher the rigidity, the less compliant the membrane is, and hence less efficient for propagating ultrasound energy. This is important to consider in the design of HiFFUTs. Note that when specifying the membrane diameter, this does not include the side-wall geometry. Also, the operating mode frequency is calculated in terms of kHz, and so is presented to three decimal places. The estimator is provided below, followed by the supplementary information important for the design and fabrication of HiFFUTs.

**Estimator of HiFFUT Operating Frequency**

| | |
|---|---|
| HiFFUT Membrane Diameter (mm): | |
| HiFFUT Membrane Thickness (mm): | |
| HiFFUT Membrane Material: | Aluminium ▾ |
| Axisymmetric Mode of Vibration: | (0,0) ▾ |
| **Modal Frequency (kHz):** | |

Calculate Reset

Figure 1: The graphical user interface for the HiFFUT design tool coded using Javascript/HTML on the publicly available project web-page.

# 1. Electro-mechanical analysis of flexural transducers

The electro-mechanical analysis of the flexural ultrasonic transducer (FUT), the configuration of which is shown in Figure 1.1 for reference, has been extended from the research presented in the first update report.

After the results of the electro-mechanical analysis are presented, the developments in the mathematical modelling are demonstrated, utilising the convolved sinusoidal function. Finally, the analysis of the dynamic nonlinearity which has been found to exist in the response of the flexural transducer, as a result of increases in amplitudes of vibration, is shown.

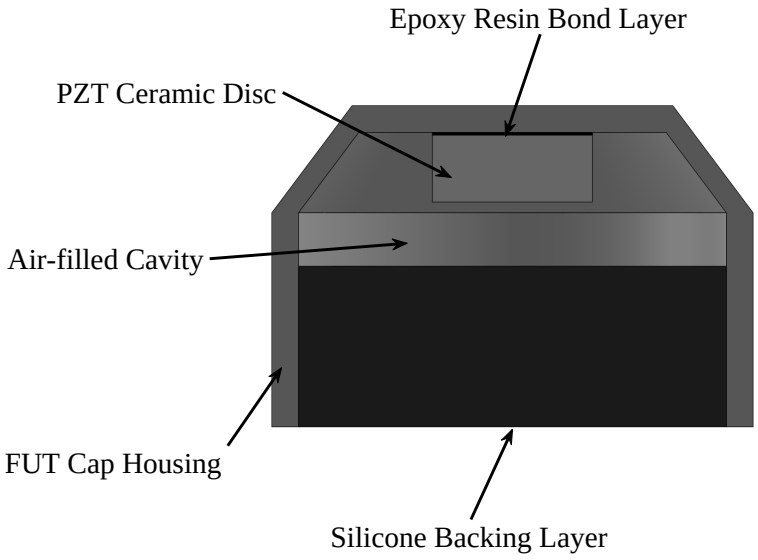


Figure 1.1: Schematic of the components of the commercial flexural ultrasonic transducer. The PZT ceramic disc is thinner in practice, but is emphasised in this schematic.

## 1.1 Experimental characterisation

Further experimental characterisation of the FUT is reported in this section, comparing the vibration characteristics of a single device measured using three different techniques, comprising an acoustic microphone (BK 4138-A-015, Brüel & Kjær Sound & Vibration Measurement A/S), laser Doppler vibrometry (LDV, Polytec OFV-5000), and through the use of another FUT as a receiver, referred to as $FUT_R$ for the purposes of this report. The experimental setup used to measure the vibration response of the FUT, showing the integration of all three measurement techniques, is shown in Figure 1.14, where a function generator is used to drive the transducer, and the vibration motion of the FUT membrane is measured by one of the three techniques described. The drive signal and the response of the FUT are both monitored by an oscilloscope.

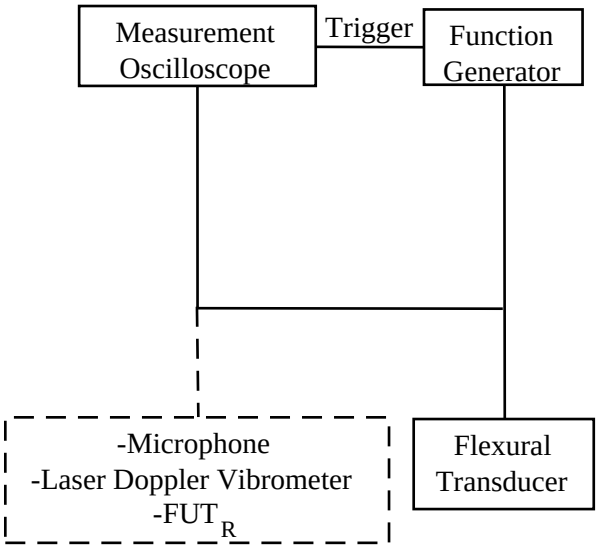


Figure 1.2: Experimental configuration used to analyse the vibration response of the FUT.

The measurement of the resonance frequency of the FUT was undertaken first. To achieve this, only a function generator and oscilloscope were used, where the amplitude-time spectra were recorded for different drive frequencies, and the fast Fourier transforms (FFTs) of these response spectra were computed. The amplitude-time spectra measured by the oscilloscope

from the function generator are shown in Figure 1.3, and the computed FFTs are displayed in Figure 1.4.

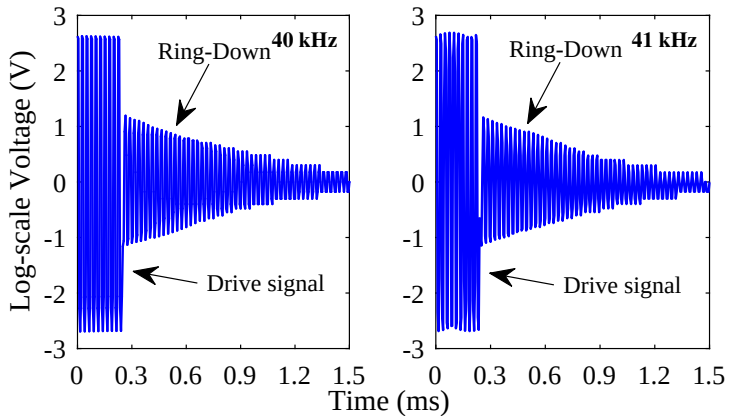


Figure 1.3: The electrical response signals measured using only a function generator and an oscilloscope, for a 10 $V_{p\text{-}p}$ and 10 cycle burst sinusoid excitation signal, for two drive frequencies close to resonance.

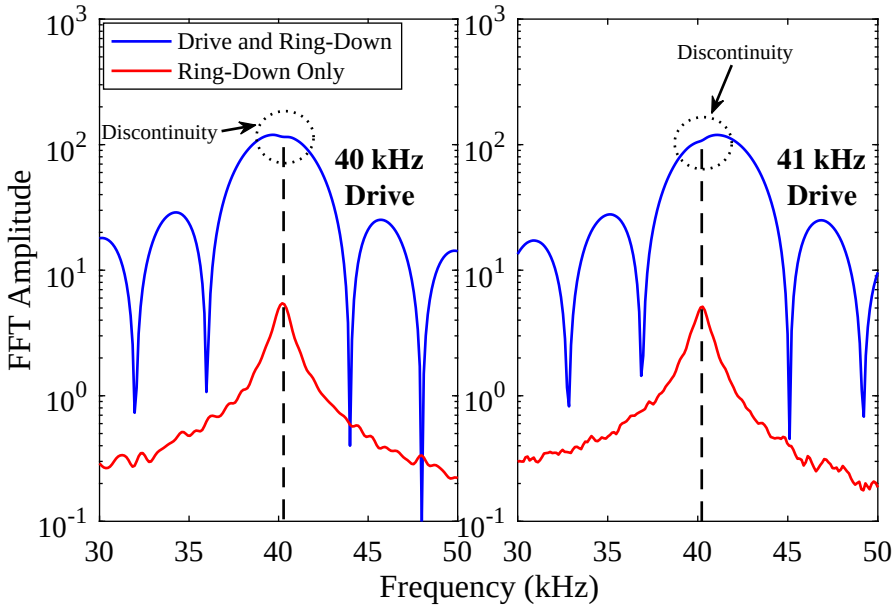


Figure 1.4: The measurement of resonance frequency of the FUT using only a function generator and oscilloscope.

Drive frequencies of 40 kHz and 41 kHz were administered to the FUT, at 10 $V_{p\text{-}p}$ and

10 sinusoidal wave cycles. The complete amplitude-time spectra were analysed for each drive condition, where a small discontinuity can be observed in the FFT of the response in each case, very close to 40 kHz. This discontinuity represents the natural resonance frequency of the FUT. The data-sheets for this type of transducer (Multicomp) state that the fundamental resonance frequency (which will be associated with the axisymmetric (0,0) mode of vibration) exists at $39.5 \pm 1.5$ kHz.

To confirm this, the vibration response of the FUT's ring-down region for each drive frequency was isolated. In previous reported research, it was shown that the FUT will ring down at its natural resonance frequency almost immediately after the drive signal is switched off. Therefore, the FFT of the exponential decay should provide a reasonably accurate computation of the resonance frequency of the FUT. The red data sets shown in Figure 1.4 show that the FFT of each isolated ring-down region corresponds exactly with the discontinuity identified in the FFT of the associated complete vibration response spectrum. This proves that through the monitoring of FUT response using an oscilloscope, most which possess an in-built capacity to provide active FFT information during experimentation, the resonance of a transducer can be rapidly measured, with great efficiency.

The characterisation of the FUT using the three aforementioned techniques was next undertaken, with the results shown in Figure 1.5. In each case, a burst sinusoidal drive signal of 10 $V_{p\text{-}p}$ and 110 cycles was applied to the FUT. Again, two drive frequencies were administered, one very close to the resonance frequency of 40 kHz, and the other off-resonance at 44 kHz.

One interesting phenomenon, which leads on from the research reported previously, is that the response spectra shown on the top plots in Figure 1.5 are almost exactly at resonance, and one characteristic phenomenon which shows this is that there is almost no over-shoot prior to steady-state. Previous research has demonstrated that for off-resonance drive signals, the vibration amplitude of the region building up towards steady-state oscillates at different amplitudes before approaching the steady-state amplitude. To emphasise this point, the vibration response of this first region prior to steady-state can be clearly observed to over-shoot the steady-state amplitude when a drive frequency of 44 kHz is applied, as shown in the bottom

plots of Figure 1.5. Each method has produced a response spectrum with similar characteristics to the others, but these response spectra can be studied and compared more closely. The FFTs of the response spectra exhibited in Figure 1.5 are shown in Figure 1.6.

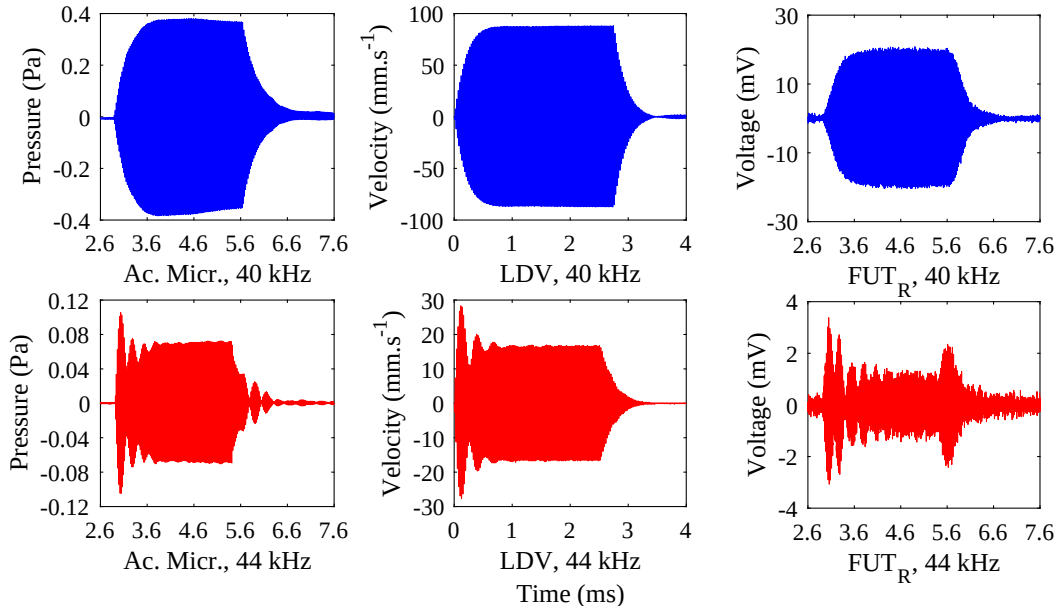


Figure 1.5: Vibration characterisation of the FUT using an acoustic microphone, LDV, and $FUT_R$, both at resonance and off-resonance.

The computed resonance frequencies in each case almost exactly overlap, showing the capability of each experimental technique to provide an accurate measurement. The FFT amplitudes have not been normalised, and are just shown as comparison between the three experimental methods. To investigate this further, the amplitude-time signals for the build-up to steady-state, and just after the steady-state region is reached, were isolated, where the experimental techniques were compared. The amplitude-time response obtained through the use of LDV was compared to the other two techniques separately, for an excitation signal with a 40 kHz drive frequency only. The results are shown in Figure 1.7.

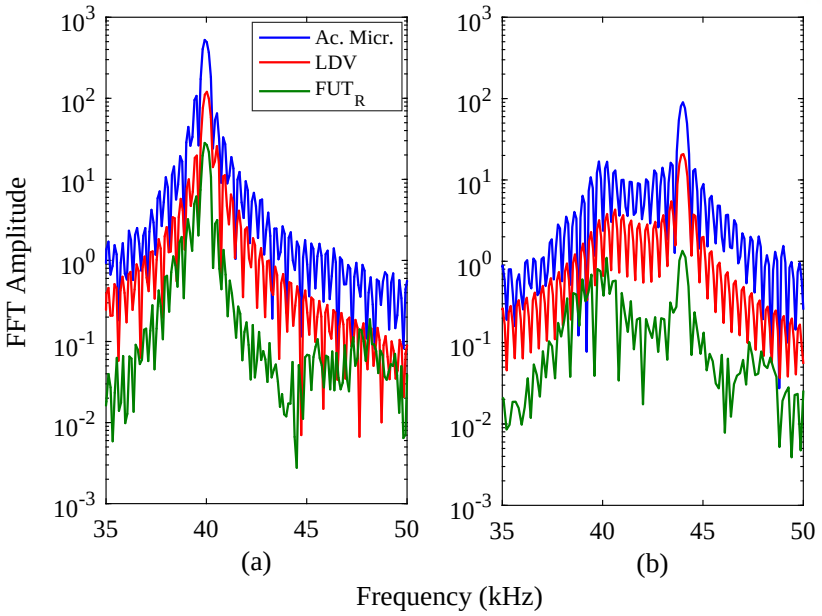


Figure 1.6: Fast Fourier transforms of the FUT response from tests conducted using an acoustic microphone, LDV, and $\mathrm{FUT_R}$, both at resonance and off-resonance.

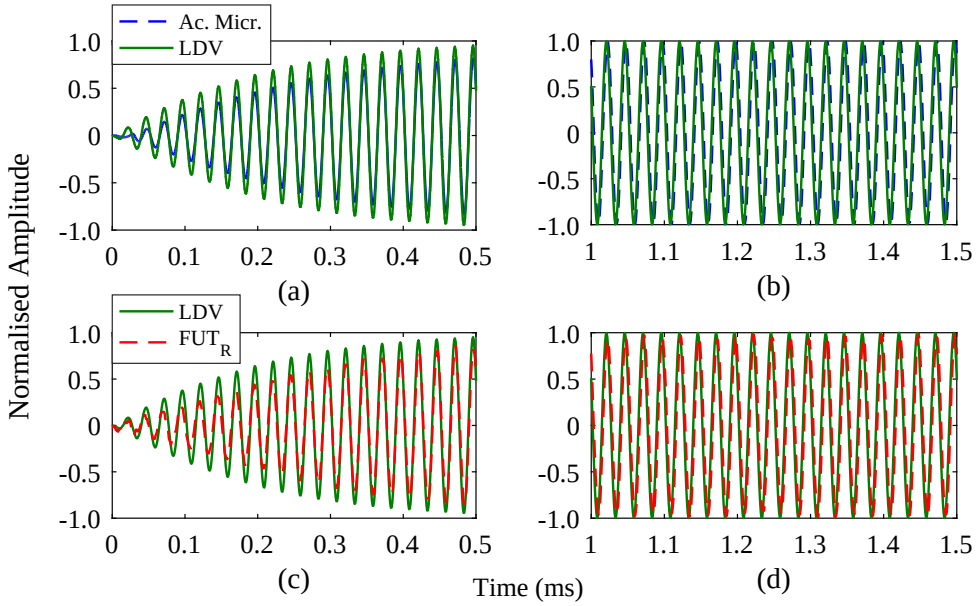


Figure 1.7: The comparison of amplitude-time responses in the build-up to steady-state, and during steady-state, for a 40 kHz drive frequency.

The results demonstrate that there is very little difference between the measured amplitude-time spectra in terms of signal shape and the change in amplitude towards steady-state. This is despite the fact that LDV is an optical-based technique, which measures the oscillation of a transducer very differently to an acoustic microphone or flexural transducer, which both rely on a compliant membrane to operate. It should be noted that the amplitude of vibration from each measurement technique is not the same, but that the normalised vibration amplitude computed for the acoustic microphone and $FUT_R$ measurements correlate reasonably closely, both being lower than that of the data obtained using LDV.

Further analysis was made on the vibration responses of the FUT for a drive signal frequency of 40 kHz. Cross-correlation is a reliable technique which can be used to assess the similarity of vibration signals. The cross-correlation of each technique combination was undertaken for the build-up towards steady-state, and part of the steady-state region, and the results are shown in Figure 1.8.

In each case, the calculated cross-correlation amplitude has been normalised. The sampling rates of both the acoustic microphone and $FUT_R$ measurements had to be switched to match that of the LDV measurements, in order to be able to apply the cross-correlation technique, and so each data set was mathematically re-sampled. The results show that there is a very high level of similarity between each technique. In the results, amplitude magnitudes of either 1 or -1 signify perfect correlation, and those magnitudes approaching zero show decreasing signal similarity. It is notable that the similarity for each technique combination marginally decreases as the vibration response approaches steady-state, but then increases again once the FUT is at steady-state.

To compare the cross-correlation spectra displayed in Figure 1.8, the absolute magnitudes of the data points were calculated, before 3$^{rd}$ order polynomials were fitted to the data. The data fits are shown in Figure 1.9.

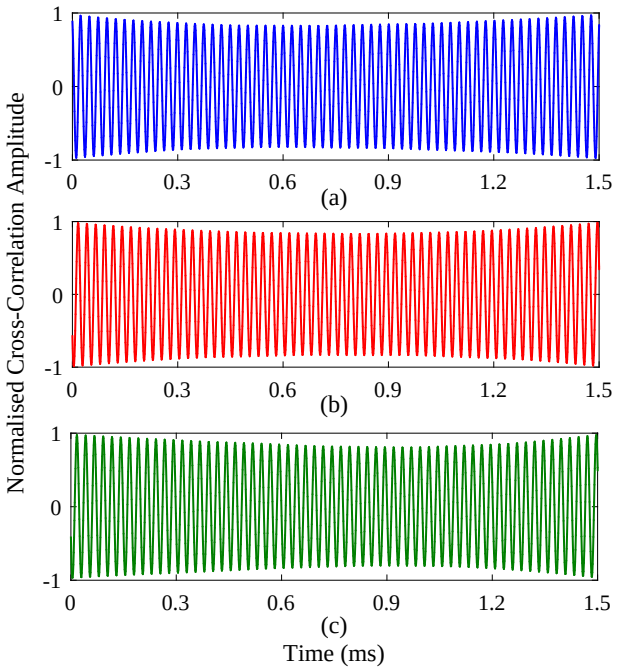


Figure 1.8: Cross-correlation of the amplitude-time responses measured using each characterisation technique, for a drive frequency of 40 kHz.

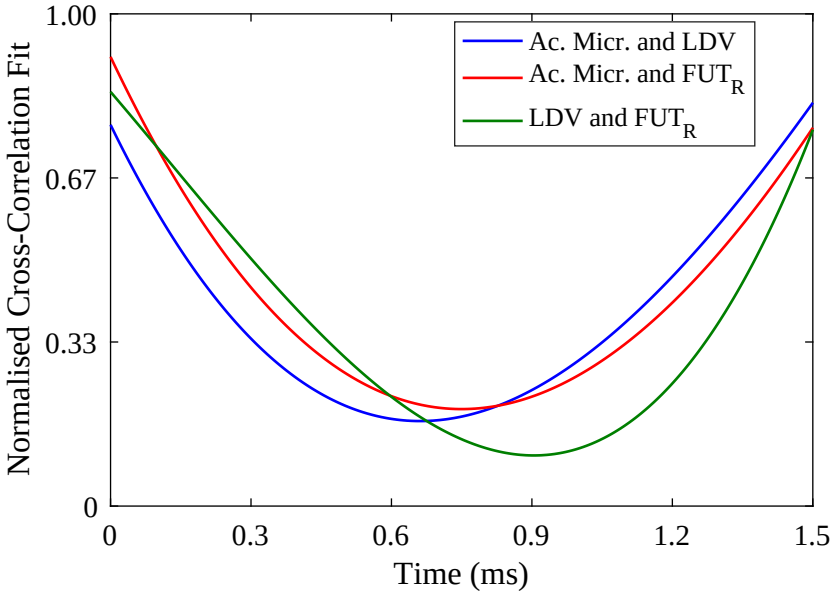


Figure 1.9: Fitted 3rd order polynomials to the absolute-magnitude cross-correlation spectra for a 40 kHz drive frequency.

The data fits shown in Figure 1.9 show the highest consistent similarity occurs in the correlation of the acoustic microphone and $FUT_R$ data. This is not unexpected, since the LDV method differs from these two techniques in terms of how mechanical vibrations are measured. LDV is an optical method, whereas the acoustic microphone and the $FUT_R$ both comprise a compliant membrane to record the vibration response of a transducer, which introduces small mass inertia effects into the response spectra, which is not the case with the LDV technique.

The electro-mechanical characterisation of the FUT presented in this section shows that there are a number of methods which can be used to accurately and reliably measure the vibration response of an FUT, and will be invaluable in the forthcoming research into HiFFUTs.

## 1.2 Mechanical analog model

The analog model, produced as a mathematical representation of the build-up of transducer response towards steady-state, was outlined in the previous update report. Further developments have been undertaken to obtain a mathematical analog which can be used to predict the amplitude and phase information, given a defined set of dynamic properties. The principal difference between this model and that described in the previous update report is the inclusion of the convolution of the sinusoidal signal with a Heaviside step function. The derivation provided previously relies upon the superposition of a natural decay signal with a sinusoidal wave.

As a reminder, the graphical schematic of the transducer is shown in Figure 1.10, where $M$ represents the vibrating mass of the transducer, $K$ the stiffness, and $C$ the damping factors of the system.

To reiterate, in **Stage 1**, it is assumed that the vibration response is zero from rest, until a discrete time, after which steady-state is produced, the response of which is represented in **Stage 2**. The first region is modelled as a convolution of the Heaviside step function with a sinusoidal forcing function of the form $F\sin\omega t$. The equation of motion is shown in Equation 1.1, with the initial conditions also defined and provided in Equation 1.2. The quantity $t_0$ rep-

resents the time at which the excitation signal is switched off. For Equation 1.2, the Heaviside function is zero for a time $t \leq 0$, but 1 prior to the beginning of Stage 2, upon the build up to steady-state. The solution to the equation of motion is shown in Equation 1.3 for $t \leq t_0$.

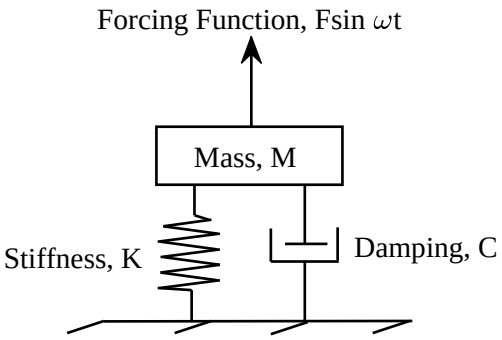


Figure 1.10: Analog schematic of the transducer.

$$M\ddot{x} + C\dot{x} + Kx = Fsin(\omega t).H(t_0 - t) \tag{1.1}$$

$$x = 0 \; and \; \dot{x} = 0 \; at \; t = 0 \tag{1.2}$$

$$For \; 0 \leq t \leq t_0, \; H = 1. \tag{1.3}$$

$$x(t) = F_+ e^{\lambda_+ t} + F_- e^{\lambda_- t} + Asin\omega t + Bcos\omega t \tag{1.4}$$

In Equation 1.4, the first two $F$ terms, the homogeneous part of the equation, represent the natural resonance of the transducer. The second part of the equation defines the forced excitation, where $\bar{E} = \sqrt{A^2 + B^2}$, the amplitude response in **Stage 1**, and is derived to be expressed in terms of $F$. The transducer is considered as an underdamped system, since it is resonant. This means that $C^2 < 4MK$, where the $\lambda$ coefficients are complex. The derived solution is of the form shown in Equation 1.5, with the phase relationship provided in Equation 1.6.

$$x(t) = F_{+}e^{-\alpha t}(cos\bar{\alpha}t + isin\bar{\alpha}t) + F_{-}e^{-\alpha t}(cos\bar{\alpha}t - isin\bar{\alpha}t) + \sqrt{A^2 + B^2}(sin(\omega t + \phi)) \quad (1.5)$$

$$tan\phi = B/A \quad (1.6)$$

The derived equation has been adapted to show its ability to produce an output amplitude-time spectrum which correlates well with experimental data. In order to generate a numerical output spectrum, Equation 1.5 can be adapted to include only the real parts of the equation. This is shown in Equation 1.7. To compare, experimental LDV data has been used, that which is shown in Figure 1.5. The comparison between the mechanical analog model fit and the experimental LDV data is shown in Figure 1.11, for drive frequencies of 40 kHz and 44 kHz.

$$x(t) = (F_{+} + F_{-})(e^{-\alpha t}(cos\bar{\alpha}t)) + \bar{E}(sin(\omega t + \phi)) \quad (1.7)$$

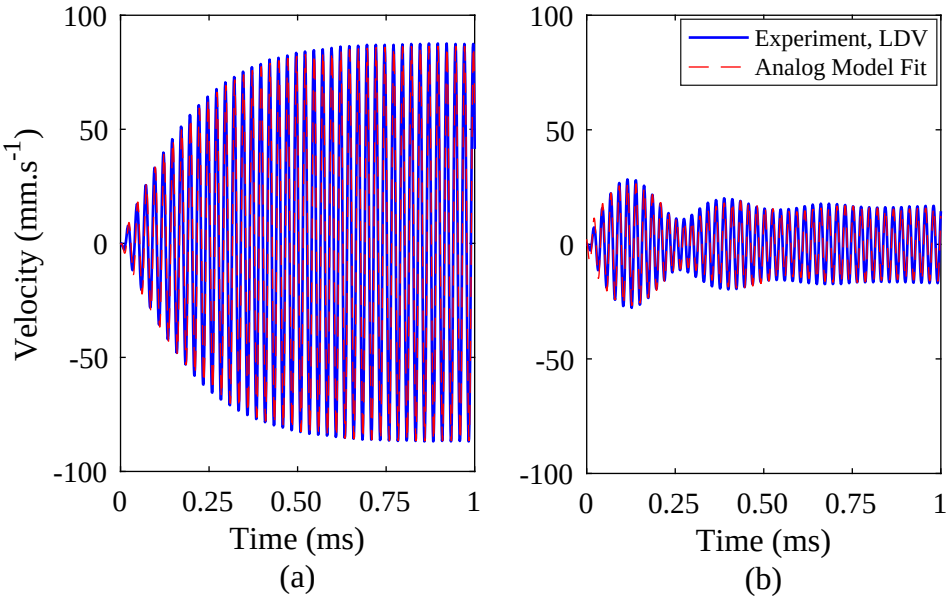


Figure 1.11: The comparison of the amplitude-time spectra from the mechanical analog model fit and experimental data obtained from LDV, for drive frequencies of (a) 40 kHz and (b) 44 kHz.

## 1.3 Nonlinearity in the dynamic response of FUTs

This study originated from the identification of apparent frequency drift in the comparison of data from tests of transducer vibration response at different excitation voltages. Nonlinearity in the dynamic response of piezoelectric-based power ultrasonic transducers has been well documented, unlike for sensors such as the flexural transducer.

The centre resonance frequency of the flexural transducer has been observed to change in response to different operating amplitudes. For clarity, an illustration of this type of generic behaviour is shown in Figure 1.12, where the deviation of resonance frequency with amplitude from a nominal centre resonance frequency, $f_N$, takes place.

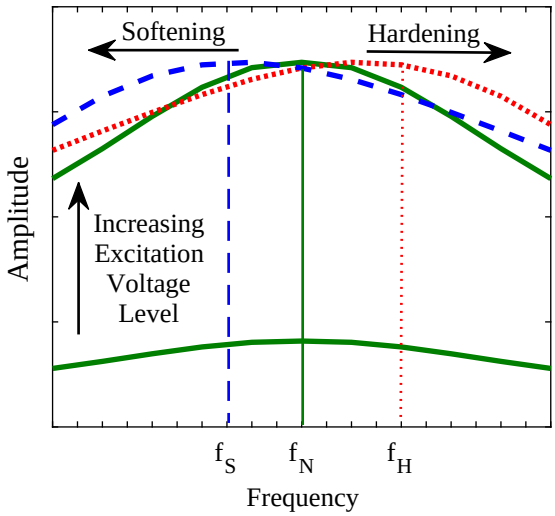


Figure 1.12: Qualitative representation of nonlinear dynamic responses, showing a softening (where $f_N$ approaches $f_S$), and a hardening (where $f_N$ approaches $f_H$) response.

Prior to laser Doppler vibrometry using a Polytec OFV-5000 laser system, the electrical characteristics of five randomly selected flexural transducers, all procured from the same supplier, were measured using an Agilent 4294A impedance gain/phase analyzer. The impedance

and phase properties as a function of frequency were obtained to identify the spread of centre frequency for nominally-identical transducers. These results are shown in Figure 1.13.

The flexural transducers are quoted with centre resonance of approximately 39.5 ± 1.5 kHz, and the measurement results exhibited in Figure 1.13 satisfy this. Interestingly, there appears to be no real difference between commercial flexural transducers marketed as receivers and those classed as transmitters. The transducers are arbitrarily numbered 1 to 5, but FUT 1 and FUT 4 are the only FUTs which were studied in more detail. From the results in Figure 1.13, there does not appear to be any consistencies which differentiate transmitters from receivers. They are hence treated identically in this research. Conductance and susceptance are electrical properties which can be used to determine the coupling coefficient, $k^2$ and the mechanical quality factor, $Q_M$, thereby enabling a more resonant device to be selected.

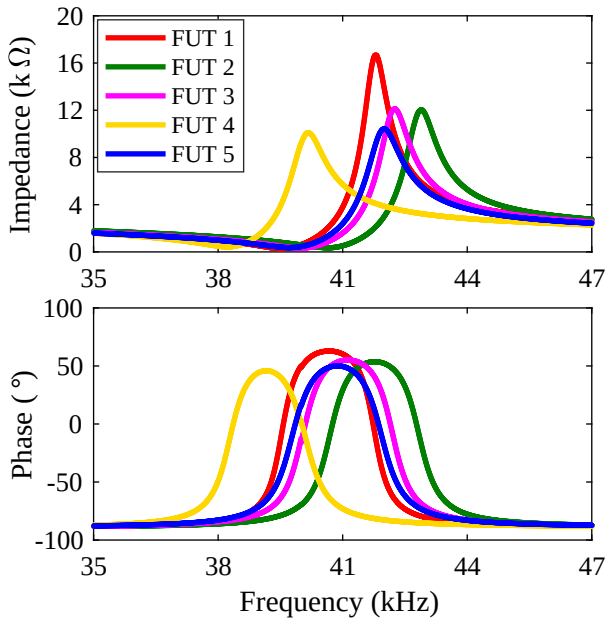


Figure 1.13: Measurements of electrical impedance and phase as a function of frequency, for five flexural ultrasonic transducers.

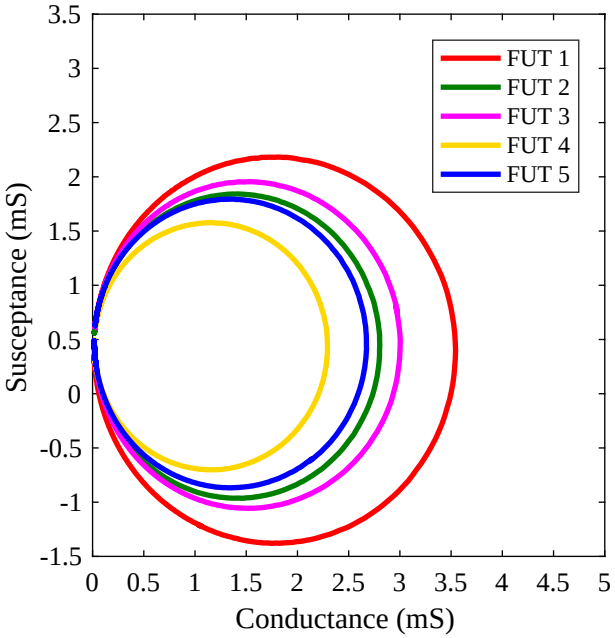


Figure 1.14: Experimental configuration used to analyse the vibration response of the flexural ultrasonic transducer.

The coupling and quality factors are both frequency-dependent, and are calculated using standard relationships shown in Equations 1.8 and 1.9.

$$k^2 = 1 - \left(\frac{f_r}{f_a}\right)^2 \tag{1.8}$$

$$Q_M = \frac{f_{rG}}{f_{2G} - f_{1G}} \tag{1.9}$$

In Equations 1.8 and 1.9, $f_r$ and $f_a$ are the resonant and anti-resonant frequencies respectively, $f_{rG}$ is the frequency of maximum conductance, and $f_{1G}$ and $f_{2G}$ are the half-maximum conductance frequencies. FUT 1 is the flexural transducer exhibiting the highest $Q_M$, and so this transducer was selected for the laser Doppler vibrometry study into the nonlinear dynamic

response characteristics. For the experiment, FUT 1 was driven with a 150-cycle burst sinusoidal signal from nominally 4 $V_{p-p}$ to 20 $V_{p-p}$, around the centre resonance frequency measured using electrical impedance analysis. The laser was focused perpendicularly to the centre of the membrane surface, and data was recorded in 100 Hz steps over a range of 1000 Hz, for sufficient measurement resolution. For the purposes of data comparison, the root mean square magnitudes of the displacement-frequency results were calculated, and compiled into the chart shown in Figure 1.15. The resonance peaks at each input excitation voltage are supported by a 3$^{rd}$ polynomial fit, which provides an indication of where the trend in the change of frequency would be directed in an experiment with even higher measurement resolution.

The results in Figure 1.15 show that there is a reduction of measured centre resonance frequency of approximately 300 Hz, in response to a change in input excitation voltage of around 16 $V_{p-p}$. This reduction can be considered as the consequence of a softening dynamic nonlinearity. All five flexural transducers were analysed in the same way, and the dynamic properties of the transducers, and the reductions in centre resonance, are summarised in Table 1.1.

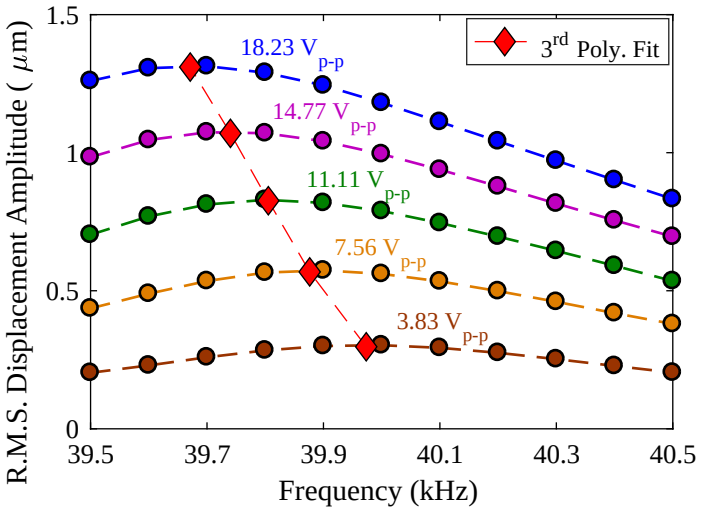


Figure 1.15: The softening nonlinear dynamic response of FUT 1 at steady-state from 3.83 $V_{p-p}$ to 18.23 $V_{p-p}$, where the dashed lines show the amplitude peaks, and the red trend-line with markers indicates the 3$^{rd}$ polynomial fit.

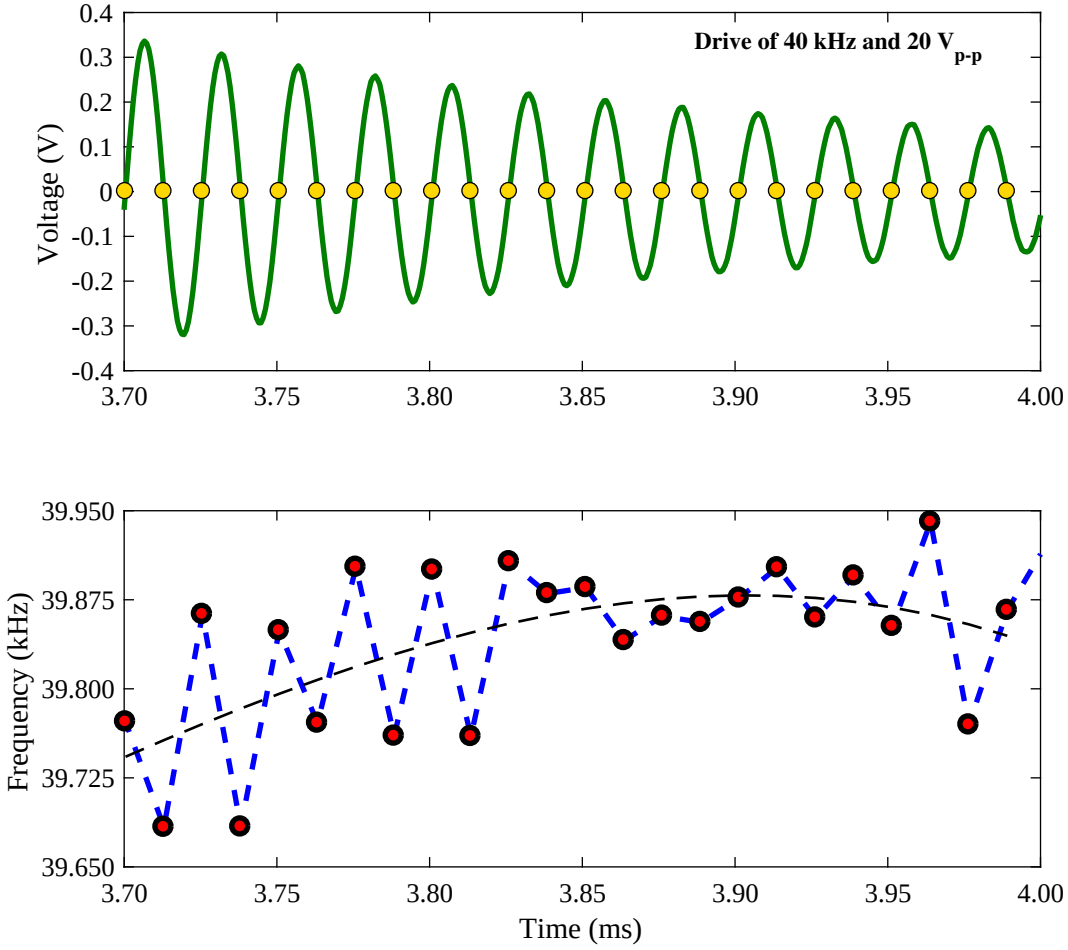


Figure 1.16: The nonlinear dynamic response of FUT 1 in the ring-down region for a 40 kHz drive frequency and 18.23 $V_{p-p}$ excitation voltage.

| | Electrical impedance analysis | | | Laser Doppler vibrometry | |
|---|---|---|---|---|---|
| **FUT** | $k^2$ | $Q_M$ | $f_r$ **(kHz)** | $f_r$ **(kHz), nom. 4** $V_{p-p}$ | $f_N$-$f_S$ **(kHz)** |
| **1** | 0.33 | 71.01 | 39.51 | 40.00 | 300 |
| **2** | 0.32 | 56.13 | 40.64 | 41.00 | 200 |
| **3** | 0.33 | 56.71 | 39.97 | 40.40 | 200 |
| **4** | 0.31 | 54.17 | 38.23 | 37.90 | 200 |
| **5** | 0.32 | 49.75 | 39.72 | 40.10 | 200 |
| **Mean** | 0.322 | 57.55 | 39.59 | 39.66 | 220 |
| **Standard deviation** | 0.007 | 7.16 | 0.88 | 0.90 | 40 |

Table 1.1: Summary of the dynamic properties of the flexural transducers measured from electrical impedance analysis and laser Doppler vibrometry.

## 1.4 Operation of FUTs at high frequency

The vibration performance of commercial FUTs (Multicomp) was analysed at high frequencies, in particular the (1,0) mode of vibration. Using the on-line design tool for this transducer configuration, fabricated from Aluminium, the (0,0) mode was estimated to be 40.2 kHz, the (1,0) mode predicted to be 156.6 kHz, and the (2,0) mode estimated to be 350.8 kHz. There will be a slight error in these values since exact transducer dimensions are not available, particularly the membrane thickness.

In this section, an aluminium FUT with a (0,0) mode frequency of 39.97 kHz - measured through electrical impedance analysis - was used. First, electrical impedance analysis using an Agilent 4294A Impedance Gain/Phase Analyzer was conducted to attempt to validate these predicted mode frequency values. Impedance-frequency and phase-frequency spectra were produced, and are shown in Figure 1.17.

The results show the (0,0) mode to exist at 39.97 kHz, the (1,0) at 176.36 kHz, and (2,0) at 318.76 kHz. Although not precise, these magnitudes are relatively close to those predicted by the on-line design tool. It should be noted that for even very minor changes to the dimensions, a much closer correlation can be achieved. It is therefore likely that dimension measurement error is a significant factor in the estimation of all modal frequencies. For example, the estimated dimensions applied in the design tool were a cap membrane diameter of 10 mm, and a cap membrane thickness of 0.4 mm. These values yield the modal frequencies provided above. By only changing the cap membrane thickness by 0.05 mm, to 0.45 mm, the frequency of the (1,0) mode is predicted by the on-line design tool to be 176.13 kHz, almost exactly the same as that measured by electrical impedance analysis, as shown in Figure 1.17.

Based on this information, an investigation was performed to determine whether a commercial FUT could be operated at a higher order axisymmetric mode of vibration, with the vibration performance measured. An acoustic microphone (BK 4138-A-015, Brüel & Kjær Sound & Vibration Measurement A/S) was first used to characterise the response at the (0,0)

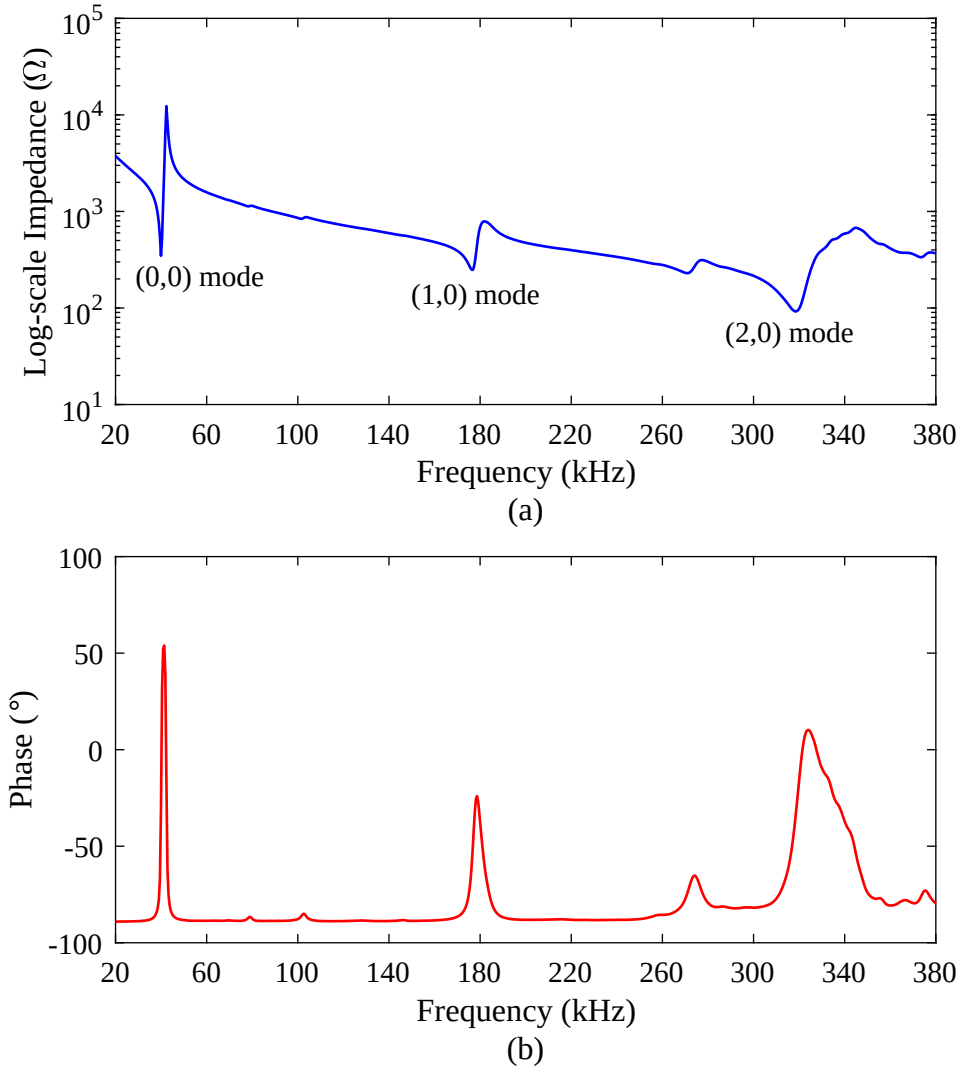


Figure 1.17: The identification of the axisymmetric modes of vibration of the FUT from electrical impedance analysis, showing (a) impedance-frequency, and (b) phase-frequency spectra.

and (1,0) modes, after which FFTs were calculated using OriginLab® . It was not possible to detect the (2,0) mode of vibration using this method. All experiments subsequently outlined in this section were conducted with burst sinusoidal input signals with 150 cycles, at 10 $_{\text{p-p}}$, with a trigger interval of 20 ms, and 1024 averages defined on the measurement oscilloscope. The results are shown in Figure 1.18.

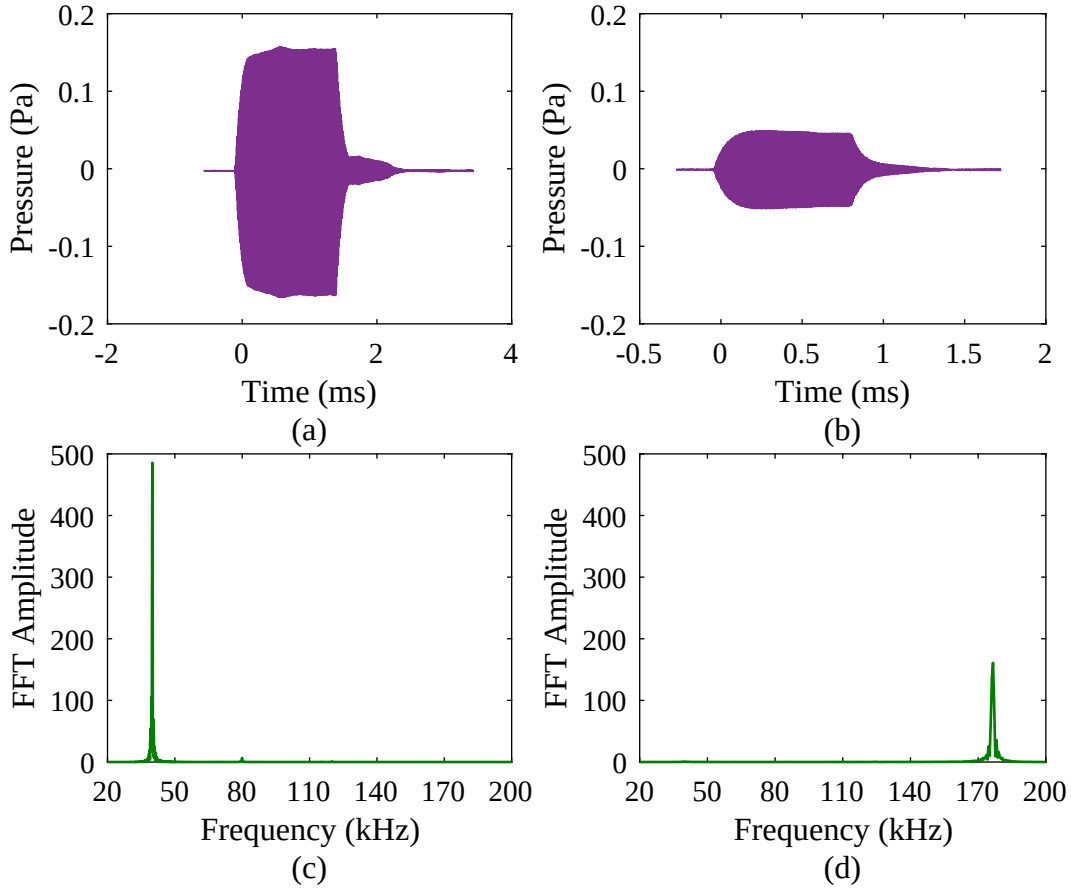


Figure 1.18: The vibration responses of the axisymmetric modes of vibration of the FUT from acoustic microphone measurements, showing (a) the pressure-time response of the (0,0) mode, (b) the pressure-time response of the (1,0) mode, (c) the FFT spectrum of the (0,0) mode, and (d) the FFT spectrum of the (1,0) mode.

The results clearly show the ability of the acoustic microphone to reliably detect the vibration of the FUT at both (0,0) and (1,0) modes of vibration, at frequencies very close to those

estimated using the on-line design tool and measured through electrical impedance analysis. The vibration response of the ring-down region only for each mode of vibration is shown in Figure 1.19, showing consistency with the results produced for the complete response spectrum in each case.

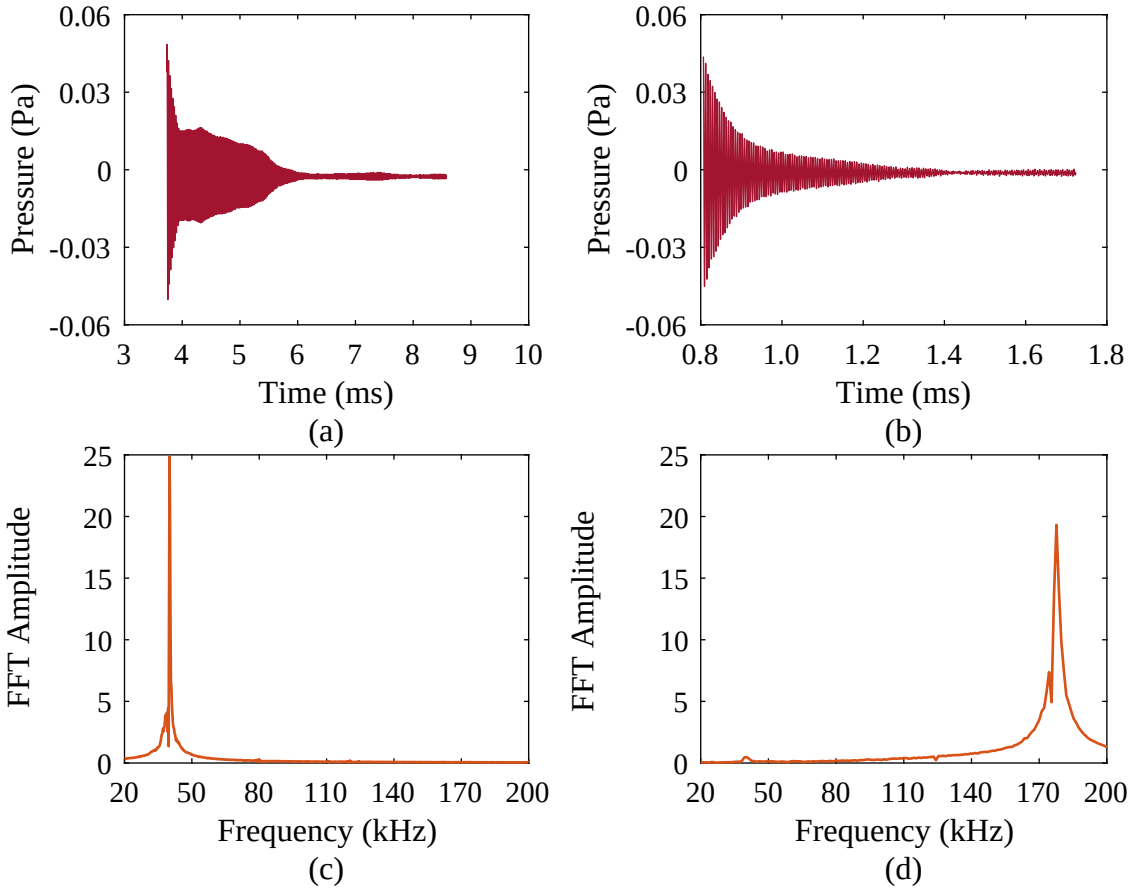


Figure 1.19: The identification of the ring-down responses of the axisymmetric modes of vibration of the FUT from acoustic microphone measurements, showing (a) the pressure-time response of the (0,0) mode, (b) the pressure-time response of the (1,0) mode, (c) the FFT spectrum of the (0,0) mode, and (d) the FFT spectrum of the (1,0) mode.

Since HiFFUTs will be used likely in conjunction with other HiFFUTs, the ability of the FUT transmitting signal to be detected by another FUT at high frequency was investigated. A second FUT was selected, with a (0,0) mode frequency of 39.51 kHz, as measured by electrical

impedance analysis. The results of this experiment are shown in Figure 1.20.

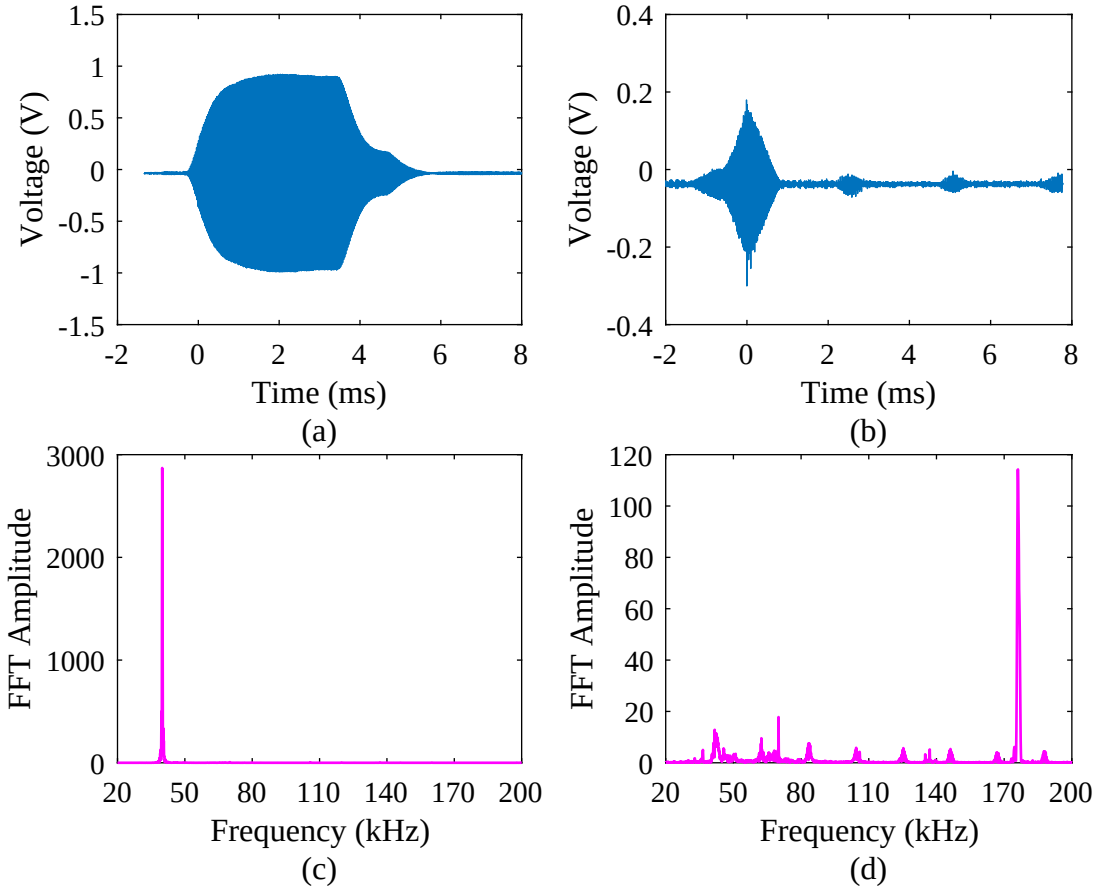


Figure 1.20: The vibration responses of the axisymmetric modes of vibration of the FUT from a FUT used as a sensor, showing (a) the pressure-time response of the (0,0) mode, (b) the pressure-time response of the (1,0) mode, (c) the FFT spectrum of the (0,0) mode, and (d) the FFT spectrum of the (1,0) mode.

The ability of the FUT to detect high frequency vibration has been demonstrated, and the results are in reasonable agreement with those obtained using the acoustic microphone technique. However, it was again not possible to record a high-quality (2,0) measurement. By significantly increasing the gain of the amplifier used in the FUT-to-FUT setup, the vibration response shown in Figure 1.21 could be detected, but further work in this area is necessary. A laser Doppler vibrometer would be able to detect the (2,0) mode with little difficulty, but

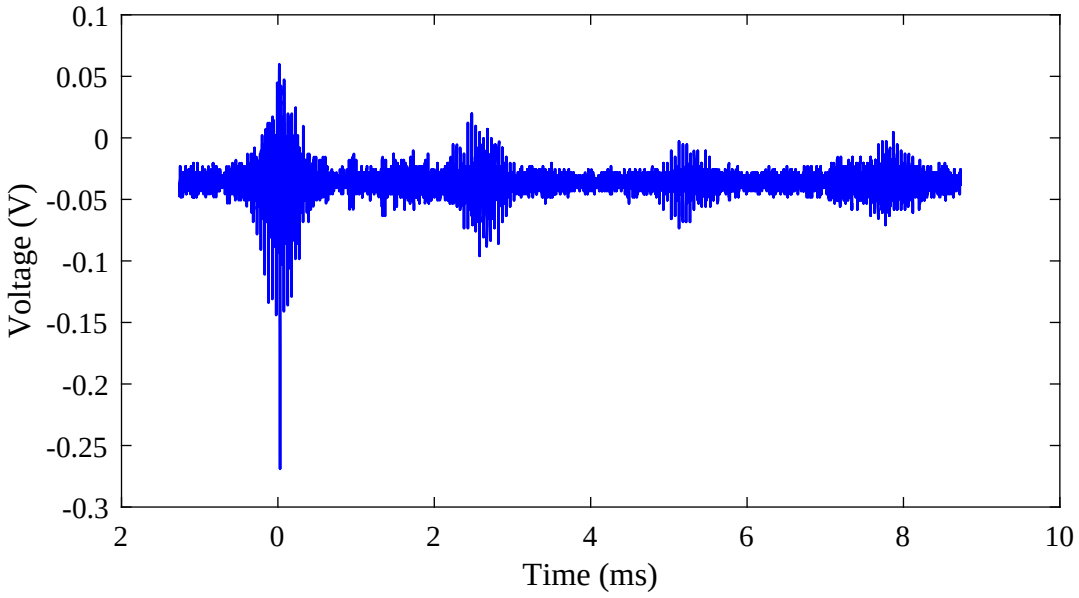


Figure 1.21: The suspected (2,0) mode detected with a FUT, through the application of very high amplifier gain, and by driving the transmitting FUT at 318.76 kHz.

a laser Doppler vibrometer would not be used in practical application. Hence, strategies for ensuring higher order modes, and high frequencies, can be effectively measured by HiFFUTs is important.

An effort was made to reduce the electrical noise in the measurement setup through grounding. The experiment was repeated using the same two FUTs. The experimental parameters, including excitation voltage and number of cycles was set to be identical to the previous experiments, and the FUTs were separated by 500 mm. The results are shown in Figure 1.22.

Each plot shows the spectrum obtained by applying the designated driving frequency. The plots shown on the left-hand side are the results of those tests conducted using the exact resonance frequencies identified through electrical impedance analysis. The plots on the right-hand side are those produced using results obtained from the on-line estimator tool used to predict the axisymmetric mode frequencies. As a reminder, the cap membrane thickness was estimated using the on-line tool, and so there is a disparity between the plots for each vibration mode. The cap thickness was modified in the on-line estimator tool until the build-up to steady-state

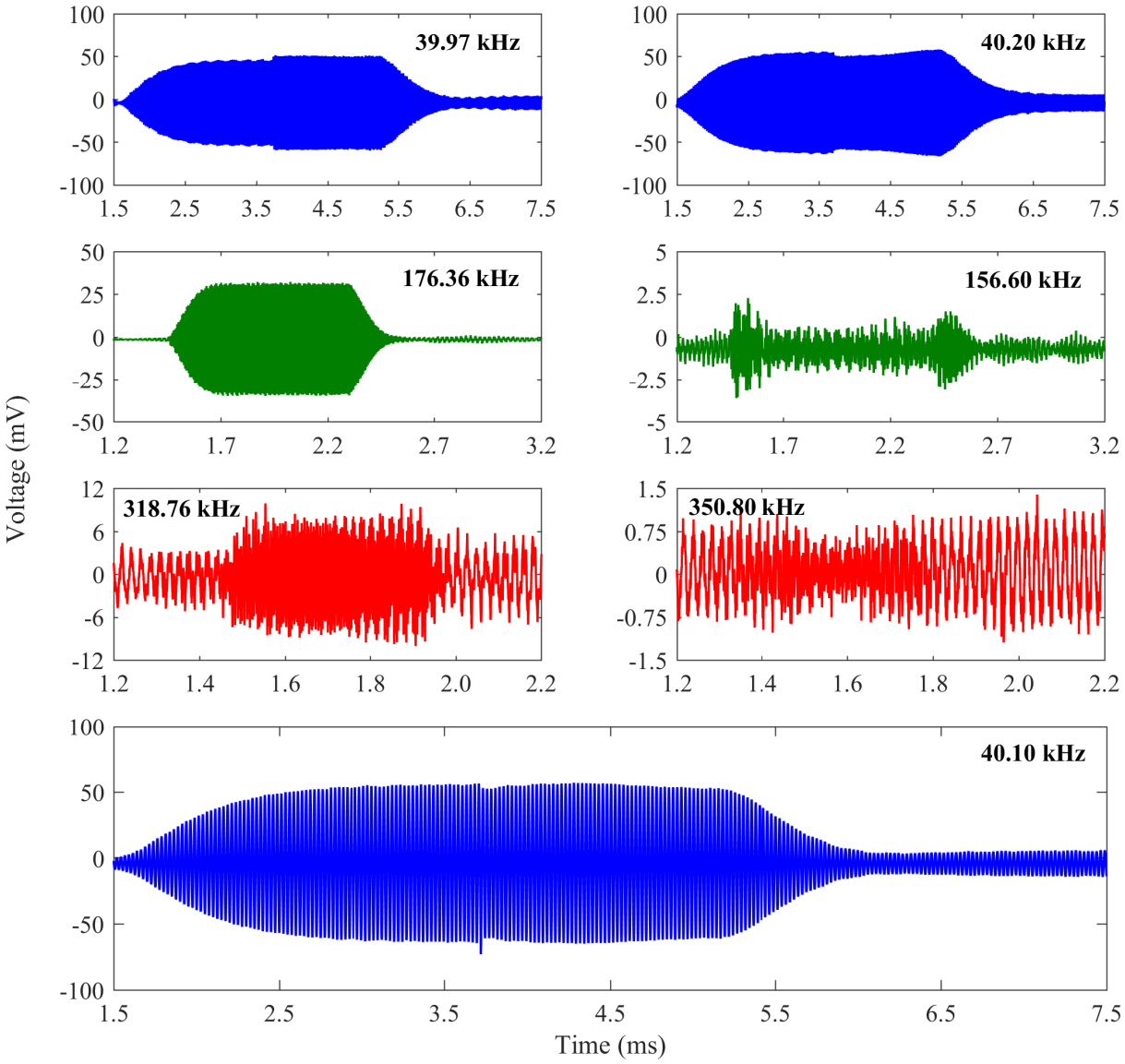


Figure 1.22: Axisymmetric modes detected with a FUT through grounding, showing the (0,0) mode in blue, (1,0) mode in green, and the (2,0) mode in the red plots.

for the (0,0) mode displayed minimal over-shoot of vibration amplitude. The result for this is shown in the bottom plot of Figure 1.22, and is at 40.1 kHz, corresponding to a cap membrane thickness of 0.39885 mm, very close to the 0.40 mm thickness specified originally. The cap membrane diameter was maintained as 10 mm throughout, but even sub-millimetre modifications to this dimension would cause a change in the predicted resonance frequencies, perhaps closer to those measured using electrical impedance analysis.

These experiments have shown the sensitivity of the resonance frequencies of the FUT to the FUT component dimensions and materials. There remains a significant amount of electrical noise in the plots of the (2,0) mode, shown in red in Figure 1.22, but there is evidence of the mode of vibration with reduced noise compared to the results shown in Figure 1.21. Furthermore, the on-line estimator tool has been used with a degree of success, as it is able to predict the resonance frequency of the (0,0) mode with reasonable accuracy, although there are minor discrepancies with respect to the resonance frequencies of the higher order modes.

This section has demonstrated the capability of FUTs to transmit and detect high frequencies, significantly above 50 kHz, but further study is required to improve the quality of the detected signals, whilst ensuring the devices will be able to operate at high pressure and temperature levels.

# 2. Pressure and Temperature Vessels

The pressure vessel design, shown in Figure 2.1 from computer aided design (CAD), was submitted to *Gilwood (Fabricators) Company Ltd.*, for manufacture, and the fabrication of this vessel is now in progress, after some discussions. The design provides capacity for both gas and liquid at high pressure, around 200 bar, and high temperature, up to 300℃, should either be required.

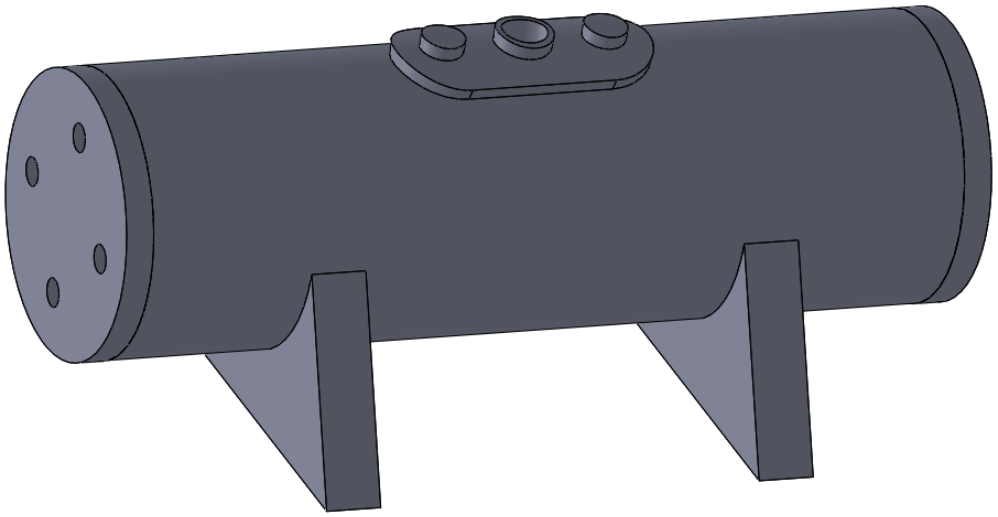

Figure 2.1: The final pressure vessel design, a variation of which is being manufactured by Gilwood (Fabricators) Company Ltd.

Other technical details and dimensional specifications are provided in the previous update report, with minor modifications where necessary made by the manufacturer's of the pressure vessel, to ensure compliance with the Pressure Equipment Directive.

# 3. Summary and Next Steps

The on-line design tool has been developed and is ready for use, and the electro-mechanical vibration behaviour of a commercial flexural ultrasonic transducer has been studied in depth, with some results now reported in the academic literature. These results have direct relevance to the design and operation of the HiFFUTs in this project. Also, most of the materials required for the laser-welding manufacture of flexural transducers have been acquired, with experimental research scheduled to commence in the final quarter of 2017. Finally, a suitable pressure vessel design has been negotiated with a supplier and is in production. The immediate next steps for this research are outlined in the following list, with the updated Gantt chart shown in Figure 3.1.

1. Continue to develop HiFFUT design strategies for the projection and detection of high frequencies.
2. Expand what I have provided on-line by providing guidelines for pressure and temperature considerations, and accounting for compliance in the HiFFUT membrane.
3. Further investigation of laser welding of titanium for transducer cap fabrication.
4. Fabrication of a laser-welded flexural transducer using the titanium caps, with BiT piezoceramic driver, followed by a characterisation process comprising measurement of electrical and dynamic properties of the transducer as a function of temperature where possible.
5. Assemble and test the pressure vessel.
6. A report on the influence of bonding pressure level on the performance of flexural transducers.
7. Begin candidate transducer designs for operation in pressurised environments, around 200 bar.

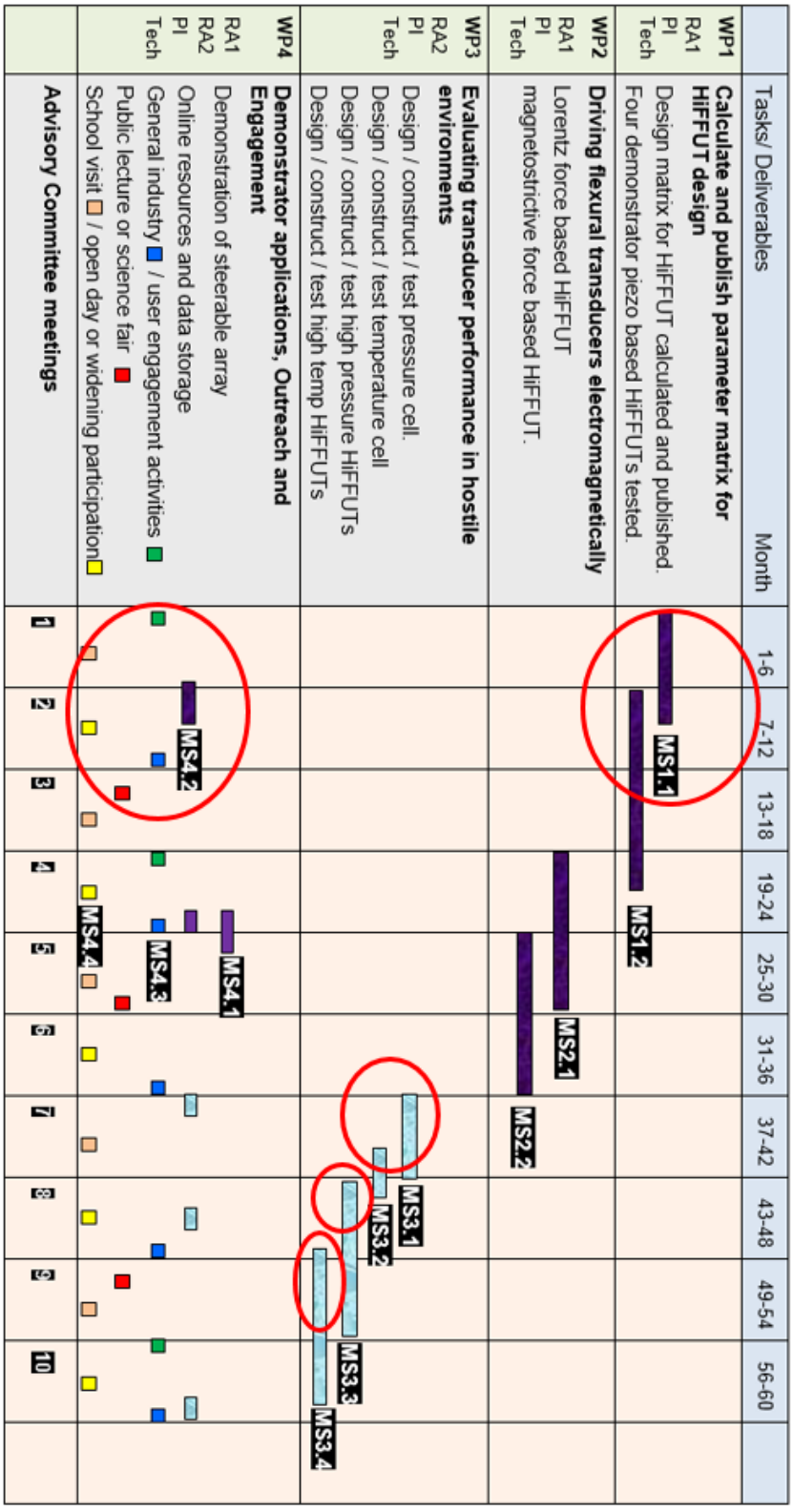


Figure 3.1: Gantt chart, indicating the areas in which the current research has addressed.

# 4. Acknowledgements


- Engineering and Physical Sciences Research Council (EPSRC) Grant No. EP/N025393/1.
- Dr Susan Burrows, University of Warwick, for advice on adhesives.
- Jonathan Harrington, University of Warwick, for component fabrication.
- Mareike Herrmann, University of Warwick, for assistance with laser cutting.
- Dr Foz Hughes, University of Warwick, for advice on adhesives.
- Dr Lei Kang, University of Warwick, for advice on modelling and experimental testing.
- Prof Mark Newton, University of Warwick, for assistance with laser cutting.
- Prof George Rowlands, University of Warwick, for assistance with analytical modelling.

**Link to grant information (Grants on the Web, EPSRC)**

gow.epsrc.ac.uk/NGBOViewGrant.aspx?GrantRef=EP/N025393/1